Analyst

ROYAL SOCIETY OF CHEMISTRY

PAPER

View Article Online
View Journal | View Issue

Cite this: *Analyst*, 2025, **150**, 887

Molecularly imprinted electrochemical sensor to sensitively detect tetramethylpyrazine in Baijiu

Yating Rui,[a] Jianfeng Wu,[b] Qunyong Tang,[b] Juan Pu,[c] Wanpeng Wang [c] and Shou-Nian Ding *[a]

Tetramethylpyrazine (TMP) is a compound known for its natural health benefits, but current detection methods for TMP are overly expensive and time-consuming. In this study, we developed functional materials with TMP molecular recognition properties using molecularly imprinted technology. As TMP does not produce electrochemical signals in the detection potential range, hexacyanoferrate was selected as a redox probe, combined with the highly conductive polymer PEDOT:PSS to enhance electrode conductivity. When coupled with the TMP-specific functional materials prepared through molecular imprinting, an electrochemical sensor specifically recognizing TMP was successfully developed, and this was confirmed through characterization techniques such as ultraviolet spectroscopy and scanning electron microscopy. Additionally, the crucial experimental parameters were optimized for improved performance. Under optimal conditions, the use of differential pulse voltammetry (DPV) to measure the peak currents of hexacyanoferrate showed a linear relationship with TMP concentrations from 0.50×10^{-6} to 5.00×10^{-3} M, achieving a detection limit of 2.1×10^{-7} M. This method proved effective for quantifying TMP in Baijiu samples, demonstrating good precision with relative standard deviations (RSD) ranging from 2.71% to 3.28%, and recovery percentages between 95.77% and 101.88%. These results indicate the potential of the molecularly imprinted polymer (MIP) sensor for accurately measuring TMP in actual samples.

Received 21st December 2024,
Accepted 19th January 2025

DOI: 10.1039/d4an01559b

rsc.li/analyst

Introduction

Baijiu, as one of traditional Chinese beverages, is an alcoholic drink that contains a rich array of flavor compounds.[1,2] The distinctive fragrance of Baijiu arises from the combination and superimposition of these compounds.[3] Despite the passage of millennia, its allure remains undiminished. Tetramethylpyrazine (TMP), commonly referred to as ligustrazine, is a pyrazine substance that has garnered considerable attention within the research community. It serves as a crucial compound of the aroma profile of Baijiu, distinguished by its roasted and sweet attributes.[4]

TMP was first derived from the traditional Chinese medicinal herb, Chuanxiong (Szechuan Lovage Rhizome) as an active alkaloid.[5] TMP is a six-membered cyclic compound with heteroatoms, and features methyl groups on each carbon atom of the pyrazine ring.[6] It holds potential for treating cardiovascular and cerebrovascular disorders. The Maillard reaction and microbial synthesis are the two main methods for producing TMP. In the production process of Baijiu, specifically, TMP is produced by microbial synthesis during qu (starter culture)-making and fermentation, while production by Maillard reaction tends to occur during distillation.[7] The content of TMP in Baijiu is related to raw materials used and the brewing process, and the content of TMP in sauce-flavored Baijiu is often higher.

TMP exhibits a wide range of pharmacological actions in the treatment of various cardiovascular diseases, including atherosclerosis and hypertension.[8–10] Additionally, TMP demonstrates significant antitumor effects. TMP can be used in conjunction with chemotherapeutic agents to increase their effectiveness and reduce the side effects of chemotherapy.[11] TMP also exhibits significant positive effects against central nervous system diseases.[12] For example, damage to dopaminergic neurons can be inhibited by TMP.[13] Furthermore, TMP possesses anti-oxidant and anti-apoptotic properties, and has demonstrated a certain efficacy in mitigating alcohol-induced liver injury.[14,15]

Currently, various methods have been reported for the detection of tetramethylpyrazine, primarily including techniques such as ultra-performance liquid chromatography coupled with tandem mass spectrometry (UPLC-MS/MS) or gas chromatography flame ionization detector (GC-FID) systems.[16,17] However, these technologies require expensive equipment and lengthy procedures, which can be a limitation in some cases.[18,19] Therefore, it is necessary to develop a new detection methodology for TMP.

[a]*Jiangsu Province Hi-Tech Key Laboratory for Biomedical Research, School of Chemistry and Chemical Engineering, Southeast University, Nanjing 211189, China. E-mail: snding@seu.edu.cn*
[b]*Jiangsu King's Lucky Brewery Joint-Stock Co., Ltd, Lian Shui 223411, China*
[c]*Lian Shui Peoples Hospital, Huaian 223400, China*

Molecular imprinting has developed as an important method for the preparation of polymeric materials with high selectivity. Due to its excellent long-term stability, cost-effectiveness, and simple preparation process, considerable research on this technology has been performed by many scientists engaged in sensor research and development.[20,21] Molecular imprinting technology (MIT) is a novel method specifically designed to identify specific compounds of interest. By designing a dedicated recognition site for the compound of interest, the technique enables the synthesis of corresponding artificial acceptors, called molecularly imprinted polymers (MIPs).[22,23]

A pre-polymer formulation is made up of cross-linkers, solvent, functional monomers, and template.[24–26] Following the polymerization process, the cross-linkers enhance the structural stability and integrity. After the template and solvent are eliminated, vast voids remain in the structure, which match the shape and interaction characteristics of the template molecules (target molecules).[27,28] Molecularly imprinted polymers operate through a 'lock and key' mechanism that enables selective binding to target molecules.[29]

The advantages of this technology include straightforward preparation, high selectivity, and robustness across various conditions.[30–32] Due to the economic viability and efficient target recognition capabilities of MIPs in complex environmental matrices, they are particularly appealing for sensor applications.[33,34] The combination of electrochemical methods with MIT can enhance surface adsorption and electrocatalytic effects, thereby increasing the sensitivity and specificity for target analytes.[35,36] However, the detection of target substances with weak electroactivity often requires the assistance of external electroactive materials, such as the selection of hexacyanoferrate as a redox probe for the sensor.[37,38]

Herein, we applied MIT combined with electrochemical sensing analysis to efficiently detect TMP. There are various advantages to electrochemical analysis, including high precision, a wide measurement range, short analysis time, minimal sample requirement, and high sensitivity and accuracy.[39,40] Additionally, due to the stability of TMP, electroactivity does not occur within the measured potential range, and therefore, we created a sensing electrode by combining a MIP and a high-conductivity polymer into a modified electrode. The quantitative principle is that TMP is specifically recognized and occupies the imprinted cavities, elevating the impedance of the sensor system, which in turn causes an effective reduction of the hexacyanoferrate sensing signal. This innovative approach enhances the detection capability and specificity for TMP, paving the way for more reliable analytical applications.[41]

Materials and methods

Reagents

2,3,5,6-Tetramethylpyrazine, 2-acetylpyrazine (2-ACE), acrylamide (AA), 2,2′-azobis (2-methylpropionitrile) (AIBN), and potassium chloride were obtained from Aladdin. Poly(3,4-ethylenedioxythiophene)-poly(styrenesulfonate), 3% in H_2O (PEDOT:PSS), was obtained from Shanghai Meryer Biotechnology Co., Ltd. Potassium ferricyanide and potassium ferrocyanide were received from ShangHai Peak Chemical Reagent Co., Ltd. Disodium phosphate dodecahydrate ($Na_2HPO_4{\cdot}12H_2O$) was provided by Sinopharm Chemical Reagent Co., Ltd. Sodium dihydrogen phosphate (NaH_2PO_4), methacrylic acid (MAA), ethylene glycol dimethacrylate (EGDMA), chitosan (CS), 2,3,5-trimethylpyrazine (tri-TMP), and ethyl lactate were acquired from Macklin, and pyrazole was purchased from Maya Reagent. Various phosphate buffer solutions with different pH values were prepared by mixing sodium dihydrogen phosphate solution (0.2 M) and disodium hydrogen phosphate solution (0.2 M), and the pH levels were validated using pH strips. Double-distilled water was used during the experiments. None of the chemical reagents underwent further purification.

Baijiu samples

Three types of Baijiu were selected, with different acidity and alcohol content, from Jiangsu King's Lucky Brewery Joint-Stock Co., Ltd. Samples were labeled J1, J2, and J3.

Apparatus

The ultraviolet (UV) spectrum was recorded by a UV-Vis-NIR spectrophotometer (UV-2600, Shimadzu, Japan). The zeta potential measurements were conducted with a Particle Size and Zeta Potential Analyzer (Omni, NanoBrook). The microscopic view of the prepared materials was investigated *via* a scanning electron microscope (FEI Inspect F50, America). In the three-electrode system for electrochemical testing, a glassy carbon electrode (GCE, Φ = 3 mm) was selected as the working electrode, while a saturated calomel electrode (SCE) was used as the reference electrode. A platinum wire served as the counter electrode. Differential pulse voltammetry (DPV) was conducted using a CHI660E electrochemical workstation. Electrochemical impedance spectroscopy (EIS) was performed using a CHI760E electrochemical workstation using a three-electrode system.

Preparation of molecularly imprinted polymer

Initially, 0.0681 g of TMP was utilized as the template molecule, and was combined with 0.2584 g of methacrylic acid and 0.2133 g of acrylamide as functional monomers. The three chemicals were dissolved in a dimethyl sulfoxide (DMSO) solution and stirred for 30 min at room temperature to achieve prepolymerization. The TMP-imprinted polymer was synthesized by free radical polymerization of the prepolymerization mixture, initiated by 0.12 g of 2,2′-azobis(2-methylpropionitrile) at 60 °C, with stirring for 2 h. During this process, 2.4 mL of ethylene glycol dimethacrylate was incorporated into the DMSO solution as a cross-linking agent. Throughout polymerization, TMP was integrated into the MIP *via* hydrogen bonding interactions. After polymerization, the TMP template and residual materials were removed from the MIP using ethanol, which resulted in an imprinting recognition cavity that mirrored the shape, size, and structure of TMP.

After drying, the MIP appeared as a loose white solid in block form, which was meticulously pulverized into a fine powder with the aid of a mortar and pestle, and subsequently stored. The complete removal of TMP from the imprinted polymer was confirmed through UV analysis, which revealed the disappearance at 280 nm of the characteristic absorption peak of TMP (Fig. 1B). Scheme 1A illustrates the synthesis procedures employed for the MIP. Additionally, to serve as a reliable control, a non-imprinted polymer (NIP)-modified electrode was created under identical experimental conditions but without the addition of TMP, thereby ensuring the reliability and accuracy of subsequent measurements.

Preparation of MIP/PEDOT:PSS/GCE

The GCEs were sequentially polished with 30 and 0.5 micrometer alumina powders, followed by ultrasonic cleaning with ethanol and double-distilled water. The acquired GCE was dried under nitrogen flow for further usage. First, 5 μL of PEDOT:PSS was carefully coated on the clean surface of the GCE. Then, 4 mg mL^{-1} MIP aqueous solution was mixed with a 0.5% chitosan acetate solution (2% acetic acid solution as the solvent) in a volume ratio of 4 : 1. Afterward, approximately 10 μL from a well-sonicated solution was dropped onto the modified electrode (PEDOT:PSS/GCE) surface, through which an MIP sensor (MIP/PEDOT:PSS/GCE) for TMP was successfully fabricated after being dried at room temperature. A diagram of the preparation process is shown in Scheme 1B. For comparison, NIP/PEDOT:PSS/GCE was also prepared using the same procedure.

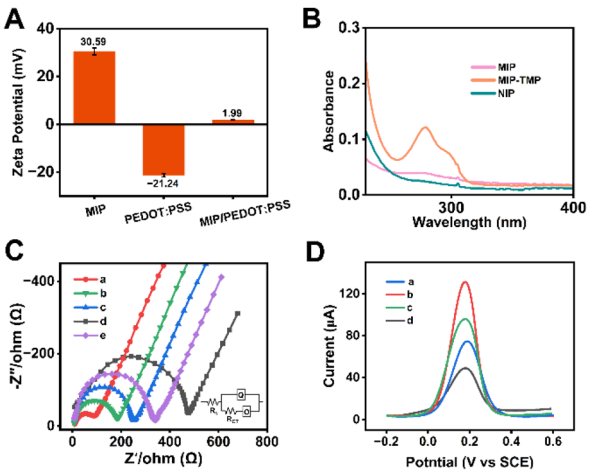

Fig. 1 (A) Zeta potentials of MIP, PEDOT:PSS, and MIP/PEDOT:PSS. (B) UV–Vis absorption spectra of MIP, MIP-TMP, and NIP solutions. (C) EIS curves for (a) PEDOT:PSS/GCE, (b) MIP/PEDOT:PSS/GCE, and (c) MIP/PEDOT:PSS/GCE after 30 min TMP binding from 0.1 μM TMP, (d) NIP/PEDOT:PSS/GCE, and (e) bare GCE in a solution containing 5 mM $[Fe(CN)_6]^{4-/3-}$ and 0.1 M KCl, where R_s, R_{ct}, Q, and O are expressed as solution resistance, charge transfer resistance, constant phase angle element, and finite layer diffusion impedance of the electrode, respectively. (D) The DPV curves of (a) bare GCE, (b) PEDOT:PSS/GCE, (c) MIP/PEDOT:PSS/GCE, and (d) MIP/PEDOT:PSS/GCE after 30 min incubation in a solution containing TMP. The DPV test environment is in a solution containing 5 mM $[Fe(CN)_6]^{4-/3-}$ and 0.1 M KCl.

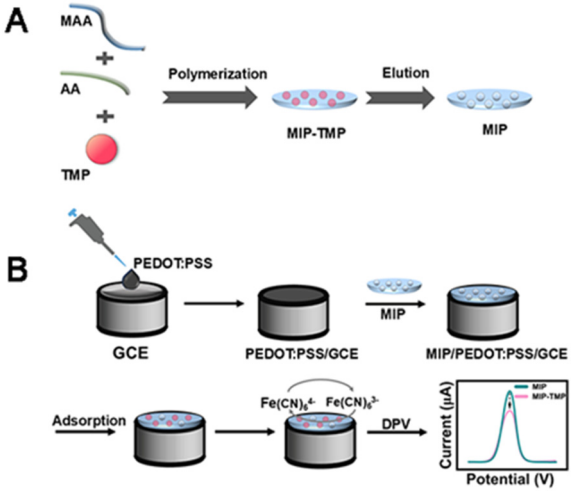

Scheme 1 (A) Schematic representation of MIP synthesis. (B) Schematic illustration of the designed MIP sensor.

Characterization

To investigate the possible formation mechanism of electrostatic interaction between the highly conductive substrate and MIP, zeta potentials were measured (Fig. 1A). The zeta potential of PEDOT:PSS was −21.24 mV, and the potential of the MIP was recorded at 30.59 mV, whereas the potential at the final MIP/PEDOT:PSS sensing interface was nearly electroneutral, at 1.99 mV. This reduction in potential assisted in minimizing nonspecific adsorption from charged substances.

MIP-TMP (before elution), MIP, and NIP were thoroughly dissolved in ethanol to achieve complete solubilization. The resulting mixtures were subsequently subjected to centrifugation at a speed of 6000 rpm for 5 min to separate the components and extract the supernatants. Following this, the UV absorption spectra of each supernatant were meticulously recorded for analysis. Fig. 1B displays the UV absorption spectra of MIP-TMP, MIP, and NIP in the 200–400 nm range. A maximum absorption peak was observed at approximately 280 nm for MIP-TMP and MIP, which was attributed to the characteristic absorption from the conjugated double bands in TMP. The UV absorption peak for MIP was particularly lower after extraction of TMP than that of MIP-TMP before extraction, while there was no characteristic TMP peak for NIP. The results revealed the successful removal of TMP in the MIP-TMP.

EIS serves as an effective method for investigating the interfacial characteristics of electrodes.[42] In the presented Nyquist plot, the diameter of the semicircle obtained from EIS measurements represents the charge transfer resistance (R_{ct}) governed by kinetics under high frequency conditions. Thus, different electrodes were immersed in 0.1 M KCl solution containing 5.0 mM $K_3[Fe(CN)_6]/K_4[Fe(CN_6)]$ by conducting EIS at 0.1–100 000 Hz. As shown in Fig. 1C, the diameter of the semicircle of the Nyquist plot in the case of the GCE modified with conductive polymer PEDOT:PSS (Fig. 1C, curve a) is smaller

than that of the bare GCE (Fig. 1C, curve e), which confirmed that PEDOT:PSS enhances the conductivity of the GCE. After further modification of the MIP, the impedance of the electrode became larger (Fig. 1C, curve b).

The MIP/PEDOT:PSS/GCE electrode was incubated for 30 min in a phosphate-buffered saline solution (pH 6.0) containing a concentration of TMP. Rebinding the template reduced the imprint cavities, resulting in an increase in R_{ct} values (Fig. 1C, curve c), because the template molecules blocked the imprinting cavities, hindering the passage of the redox probe. The R_{ct} value of NIP/PEDOT:PSS/GCE (Fig. 1C, curve d) was considerably augmented due to the modification of the non-conductive polymer, NIP, which reduced the passage of the redox probe.

The morphologies of the substrate, NIP, MIP, and the MIP soaked in a solution containing a specific concentration of TMP for 30 min were analysed by scanning electron microscopy (SEM) (Fig. 2). The surface of PEDOT:PSS exhibited slight wrinkling, but overall, it presents a relatively smooth planar structure (Fig. 2A). The surface of the NIP exhibited relatively fewer cavities (Fig. 2B), while the MIP (Fig. 2C), following the removal of the template, presents a greater number of surface recognition sites, resulting in the formation of numerous pores (Fig. 2D). After immersion in a TMP solution, the surface of the MIP solid shows a significant reduction in the number of pores. In comparison, the formation of MIP was affirmed.

The DPV curve presented in Fig. 1D indicates that the unmodified oxidation peak potential of the hexacyanoferrate solution is approximately 0.19 V. Following the modification of GCEs with PEDOT:PSS polymer, this potential decreases to approximately 0.18 V. This modification resulted in a reduction of approximately 0.01 V in the oxidation peak potential compared to the bare GCEs. Additionally, an evident increase in current value was observed, indicating enhanced electrochemical activity due to the polymer modification. However, after the application of the droplet-coated MIP mixture to form the MIP sensor, the oxidation current decreased. Furthermore, immersion in a solution containing TMP led to an additional reduction in the oxidation current. These results implied that the MIP electrochemical sensor was successfully fabricated.

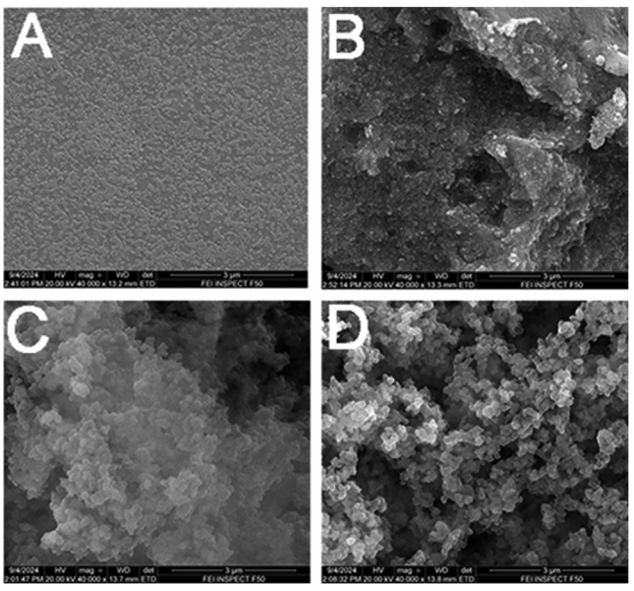

Fig. 2 SEM images of (A) PEDOT:PSS, (B) NIP, (C) MIP immersed in TMP solution, and (D) MIP.

Results and discussion

Electrochemical measurement optimization of experimental parameters

Due to the high sensitivity of DPV, subsequent quantitative detection of TMP was conducted using DPV. An initial peak current (i_0) of DPV was documented when the MIP/PEDOT:PSS/GCE as the working electrode was immersed in a 5.0 mM $K_3[Fe(CN)_6]/K_4[Fe(CN_6)]$ mixed solution containing 0.1 M KCl with a three-electrode cell. The electrode was submerged in the prepared standard concentration solution of TMP for minutes, carefully rinsed with double-distilled water to eliminate possible physical adsorbates, and dried under nitrogen. The electrode was then inserted into hexacyanoferrate solution, and the DPV was measured and recorded again, with the peak current being labeled as i_x.

The sensor's response was determined by the variation in the current of hexacyanoferrate, which was calculated as the difference between the initial current (i_0) and the current at a given time (i_x), and represented as $\Delta i_p = i_0 - i_x$. The DPV measurements were conducted over a potential range of −0.2 V to 0.6 V, with an amplitude of 50 mV and a pulse width of 50 ms. To obtain the best electrochemical performance, three variables (incubation time, the pH of the buffer solution containing a certain concentration of TMP, and MIP concentration) were individually modified while the other variables were maintained at a constant level. All optimization trials were conducted using DPV. The optimal conditions were assessed by measuring the change in oxidation current (Δi_p).

Incubation time

The template-extracted MIP/PEDOT:PSS/GCE was immersed in the analyte solution for a duration of 5–45 min. The sensor was incubated in a 10^{-6} M TMP buffer solution for different times, gently rinsed with double-distilled water, dried under nitrogen in turn, and then placed in 0.1 M KCl solution containing 5.0 mM $K_3[Fe(CN)_6]/K_4[Fe(CN_6)]$ to quantitatively measure the peak current. Fig. 3A records the difference between the oxidation peak currents before and after incubation for MIP/PEDOT:PSS/GCE. It was noted that Δi_p increased as the incubation time increased, which was attributed to the occupation of some binding sites in the MIP by TMP. A consistent response was achieved following a 30-minute immersion. Consequently, a 30 min incubation

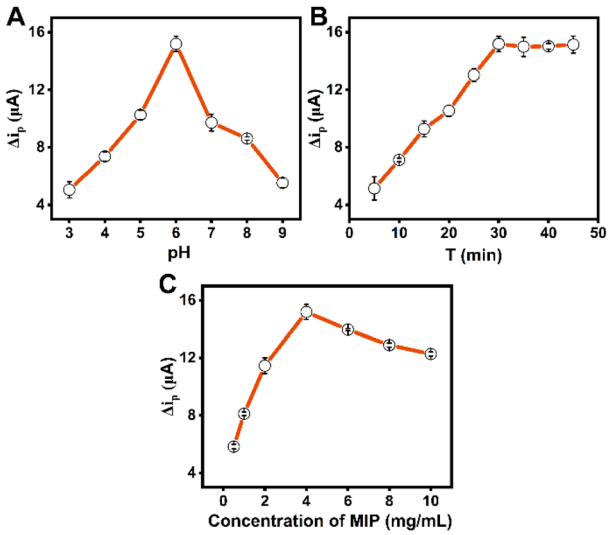

Fig. 3 Optimization of different conditions affecting the TMP extraction and determination in the MIP/PEDOT:PSS/GCE. Variation in electrode response for TMP after changing the (A) electrode incubation time, (B) TMP solution pH, and (C) concentration of MIP.

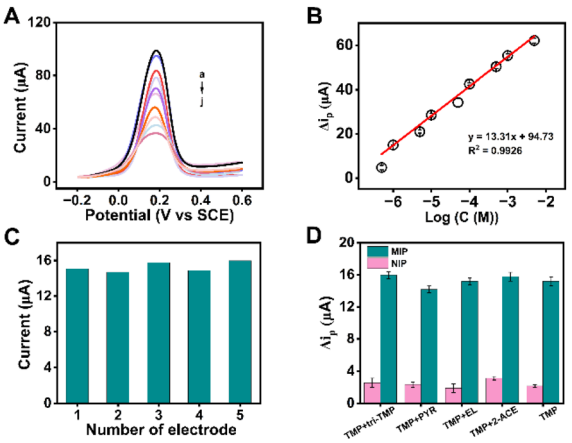

Fig. 4 (A) DPV current response of the MIP/PEDOT:PSS/GCEs to different concentrations of TMP: (a) 0, (b) 0.5 μM, (c) 1 μM, (d) 5 μM, (e) 0.01 mM, (f) 0.05 mM, (g) 0.1 mM, (h) 0.5 mM, (i) 1 mM, and (j) 5 mM. (B) Linear calibration curves of current response difference *versus* logarithm of TMP concentrations (n = 3). (C) Reproducibility of the DPV responses. (D) Specificity of the MIP and NIP sensors for mixtures of TMP (1 μM) and tri-TMP (10 μM), PRY (10 μM), EL (10 μM), and 2-ACE (10 μM), respectively. Compared to TMP (1 μM) alone.

period was established as the optimal duration for the determination of TMP.

Optimization of pH

A series of phosphate buffer solutions with pH from 3.0 to 9.0 containing a concentration of 10^{-6} M TMP was investigated, and the current response was documented. The difference in peak oxidation current (Δi_p) observed before and after the introduction of TMP gradually increased with pH values rising from 3.0 to 6.0, and subsequently declined when the pH surpassed 6.0. The highest response was recorded at a pH of 6.0. Thus, the optimal pH for the phosphate buffer solutions was established at 6.0 (Fig. 3B).

Optimization of the concentration of MIP

The amount of the MIP is an important factor affecting the sensor's recognition ability. Hence, it was necessary to optimize the concentration of MIP. MIP/PEDOT:PSS/GCEs were synthesized utilizing solutions that varied in MIP concentrations within the range of 1–10 mg mL^{-1}. As depicted in Fig. 3C, the current response exhibited a peak at a concentration of 4 mg mL^{-1}, indicating optimal performance. Beyond this concentration, the current response gradually decreased as the MIP concentration increased. Consequently, a MIP concentration of 4 mg mL^{-1} was selected because it provided the highest sensitivity for the determination of TMP, ensuring optimal detection capabilities.

Calibration curve and detection limit

To assess the practical applicability of the MIP/PEDOT:PSS/GCEs for the detection of TMP, MIP/PEDOT:PSS/GCEs were employed under optimal conditions to detect a series of TMP standard solutions, with parameters consistent with those previously mentioned. Fig. 4A illustrates the DPV curves of MIP/GCE in a potassium ferricyanide medium after incubation with different concentrations of TMP (from top to bottom: 0, 5.0×10^{-4}, 1.0×10^{-3}, 5.0×10^{-3}, 0.01, 0.05, 0.1, 0.5, 1, and 5 mM). As shown in Fig. 4A, the peak current decreased as the concentration of TMP increased, indicating that additional imprinted sites were occupied by TMP molecules. With the increase in TMP concentration, the pathways and cavities for ferricyanide to reach the GCE surface decreased, resulting in a reduction in the current change (Δi_p) in the hexacyanoferrate current value, and demonstrating a linear relationship, as shown in the calibration curve in Fig. 4B. The linear regression equation for detection of TMP is Δi_p (μA) = 13.31 × log($C(M)$) + 94.73 in the concentration range of 0.5–500.0 μM and a correlation coefficient of 0.9926. The detection limit is 0.21 μM (n = 3). Reproducibility experiments were conducted to evaluate the precision of the measurements. Among the five electrodes tested, no significant differences were observed in the hexacyanoferrate current signals, with a relative standard deviation (RSD) of 2.19% (Fig. 4C), which indicates the consistent reproducibility of the sensor.

Selectivity

The selectivity of the TMP molecularly imprinted sensor was evaluated by selecting structurally similar or coexisting interfering substances in Baijiu (2,3,5-trimethylpyrazine (tri-TMP), pyrazole (PYR), ethyl lactate (EL), and 2-acetylpyrazine (2-ACE), each at 10 μM) and TMP (1 μM) to be separately mixed. Compared with TMP (1 μM) alone, these experimental results (Fig. 4D) illustrated that the sensor was nearly unaffected by these interfering substances, which demonstrated the excellent specificity of the MIP/PEDOT:PSS/GCE sensor.

Table 1 Comparison of experimental results of GC-MS with MIP sensor (n = 3), and spiked recovery experiments with MIP sensor (n = 3)

		MIP sensor			MIP sensor		
Baijiu samples	GC-MS (μM)	Found (μM)	RSD (%)	Added (μM)	Found (μM)	RSD (%)	Recovery (%)
J1	191.83	187.49	3.04	10	201.21	2.71	101.88
J2	—	—	—	20	19.64	3.28	98.2
J3	—	—	—	30	28.73	2.97	95.77

Realistic sample analysis

The evaluation of the sensor was conducted through the quantification of TMP in actual sample solutions. The pH of various Baijiu samples significantly varied. Each sample was diluted 100 times with a phosphate buffer at pH 6. MIP/PEDOT:PSS/GCEs were immersed in these diluted solutions for 30 minutes to assess their interactions with TMP in Baijiu samples. As shown in Table 1, consistent with the results of GC-MS detection, the MIP electrochemical sensor also did not detect TMP in samples J2 and J3. The spiked recovery experiments were subsequently carried out on the abovementioned three groups of Baijiu samples, and the recoveries of the constructed sensing platform ranged from 95.77% to 101.15% (Table 1), demonstrating that this MIP sensor for TMP was highly practical, and suggesting favorable characteristics of the MIP sensor for an effective quantitative assay of TMP in Baijiu samples.

Conclusions

A novel, simple, and sensitive electrochemical sensor for the detection of TMP was constructed and then combined with molecular imprinting technology. Utilizing the high conductivity of the polymer PEDOT:PSS, a GCE was modified and then integrated with a MIP that recognized the TMP template, thereby building a MIP sensor to amplify electrochemical signals. The optimized conditions for DPV by the MIP sensors were thoroughly examined. Under established experimental parameters, the change in the oxidation current of hexacyanoferrate (Δi_p) demonstrated a linear relationship with TMP concentration, ranging from 5.0×10^{-7} to 5.0×10^{-3} M, and achieving a detection limit of 2.1×10^{-7} M.

The developed sensor exhibited excellent recognition capability and exceptional selectivity for the target molecule, even in the presence of high levels of structurally similar interfering substances. Furthermore, it demonstrated remarkable repeatability and stability. This study may offer a convenient, reliable, and cost-effective method for detecting trace amounts of TMP in the analysis of Baijiu samples. It broadens the assay for the detection of TMP.

Data availability

The data for this article are available from the corresponding author on reasonable request.

Conflicts of interest

There are no conflicts to declare.

Acknowledgements

This work was supported by the National Natural Science Foundation of China (22174015).

References

1 P. Du, G. Jiao, Z. Zhang, J. Wang, P. Li, J. Dong and R. Wang, *Fermentation*, 2023, **9**, 658.
2 G. Wang, X. Song, L. Zhu, Q. Li, F. Zheng, X. Geng, L. Li, J. Wu, H. Li and B. Sun, *Food Chem.*, 2022, **374**, 131641.
3 G. Wang, X. Li, X. Song, S. Jing, S. Meng, F. Zheng, H. Li, Z. Li, C. Shen and Y. Shen, *Food Anal. Methods*, 2022, **15**, 1606–1618.
4 Y. Liu, M. Li, X. Hong, H. Li, R. Huang, S. Han, J. Hou and C. Pan, *J. Sci. Food Agric.*, 2023, **103**, 6849–6860.
5 C. Y. Chang, C. C. Wu, P. H. Pan, Y. Y. Wang, S. Y. Lin, S. L. Liao, W. Y. Chen, Y. H. Kuan and C. J. Chen, *Exp. Neurol.*, 2023, **367**, 114468.
6 G. Li, K. S. Sng, B. Shu, Y. Wang, M. Yao and X. Cui, *Eur. J. Pharmacol.*, 2023, **945**, 175524.
7 X. Shi, S. Zhao, S. Chen, X. Han, Q. Yang, L. Zhang, X. Xia, J. Tu and Y. Hu, *Front. Nutr.*, 2022, **9**, 1004435.
8 J. R. Sheu, Y. C. Kan, W. C. Hung, W. C. Ko and M. H. Yen, *Thromb. Res.*, 1997, **88**, 259–270.
9 H. Zhang, H. Chen, X. Wu, T. Sun, M. Fan, H. Tong, Y. Zhu, Z. Yin, W. Sun, C. Zhang, X. Zheng and X. Chen, *Phytomedicine*, 2022, **96**, 153860.
10 Q. Yang, D. D. Huang, D. G. Li, B. Chen, L. M. Zhang, C. L. Yuan and H. H. Huang, *Cell. Mol. Biol. Lett.*, 2019, **24**, 17.
11 S. Yang, S. Wu, W. Dai, L. Pang, Y. Xie, T. Ren, X. Zhang, S. Bi, Y. Zheng, J. Wang, Y. Sun, Z. Zheng and J. Kong, *Front. Pharmacol.*, 2021, **12**, 764331.
12 Y. Liu, G. Yang, W. Cui, Y. Zhang and X. Liang, *Front. Pharmacol.*, 2022, **13**, 948600.
13 H. Zhao, M. L. Xu, Q. Zhang, Z. H. Guo, Y. Peng, Z. Y. Qu and Y. N. Li, *Neurol. Sci.*, 2014, **35**, 1963–1967.
14 Y. Zhou, R. Wu, X. Wang, Y. Jiang, W. Xu, Y. Shao, C. Yue, W. Shi, H. Jin, T. Ge, X. Bao and C. Lu, *Free Radicals Biol. Med.*, 2022, **179**, 301–316.

15 C. F. Liu, C. H. Lin, C. F. Chen, T. C. Huang and S. C. Lin, *Am. J. Chin. Med.*, 2005, **33**, 981–988.
16 Y. Yan, S. Chen, Y. Nie and Y. Xu, *Foods*, 2021, **10**, 441.
17 Z. Xiao, L. Zhao, L. Tian, L. Wang and J. Zhao, *Food Chem.*, 2018, **239**, 726–732.
18 W. Xu, F. Yuan, C. Li, W. Huang, X. Wu, Z. Yin and W. Yang, *J. Sep. Sci.*, 2016, **39**, 4851–4857.
19 M. L. Yola and N. Atar, *Appl. Surf. Sci.*, 2018, **458**, 648–655.
20 A. Nezhadali and R. Shadmehri, *Sens. Actuators, B*, 2013, **177**, 871–878.
21 L. Özcan and Y. Şahin, *Sens. Actuators, B*, 2007, **127**, 362–369.
22 P. Lach, A. Garcia-Cruz, F. Canfarotta, A. Groves, J. Kalecki, D. Korol, P. Borowicz, K. Nikiforow, M. Cieplak, W. Kutner, S. A. Piletsky and P. S. Sharma, *Biosens. Bioelectron.*, 2023, **236**, 115381.
23 X. He, W. Ji, S. Xing, Z. Feng, H. Li, S. Lu, K. Du and X. Li, *Talanta*, 2024, **268**, 125283.
24 H. Hrichi, M. R. Louhaichi, L. Monser and N. Adhoum, *Sens. Actuators, B*, 2014, **204**, 42–49.
25 E. Mathieu-Scheers, S. Bouden, C. Grillot, J. Nicolle, F. Warmont, V. Bertagna, B. Cagnon and C. Vautrin-Ul, *J. Electroanal. Chem.*, 2019, **848**, 113253.
26 C. Salvo-Comino, I. Rassas, S. Minot, F. Bessueille, M. L. Rodriguez-Mendez, A. Errachid and N. Jaffrezic-Renault, *Mater. Sci. Eng., C*, 2020, **110**, 110667.
27 C. Herdes and L. Sarkisov, *Langmuir*, 2009, **25**, 5352–5359.
28 S. Rahman, B. Bozal-Palabiyik, D. N. Unal, C. Erkmen, M. Siddiq, A. Shah and B. Uslu, *Trends Environ. Anal. Chem.*, 2022, **36**, e00176.
29 S. Ding, Z. Lyu, S. Li, X. Ruan, M. Fei, Y. Zhou, X. Niu, W. Zhu, D. Du and Y. Lin, *Biosens. Bioelectron.*, 2021, **191**, 113434.
30 T. Alizadeh, M. Zare, M. R. Ganjali, P. Norouzi and B. Tavana, *Biosens. Bioelectron.*, 2010, **25**, 1166–1172.
31 A. Herrera-Chacón, Ş. Dinç-Zor and M. del-Valle, *Talanta*, 2020, **208**, 120348.
32 A. Hammoud, D. Chhin, D. K. Nguyen and M. Sawan, *Biosens. Bioelectron.*, 2021, **180**, 113089.
33 W. Zhao, Y. Ma and J. Ye, *J. Electroanal. Chem.*, 2021, **888**, 115215.
34 L. Kiss, V. David, I. G. David, P. Lazăr, C. Mihailciuc, I. Stamatin, A. Ciobanu, C. D. Ştefănescu, L. Nagy, G. Nagy and A. A. Ciucu, *Talanta*, 2016, **160**, 489–498.
35 M. M. El-Wekil, A. M. Hayallah, M. A. Abdelgawad, M. A. S. Abourehab and R. Y. Shahin, *J. Electroanal. Chem.*, 2022, **922**, 116745.
36 B. Tang, H. Shi, Z. Fan and G. Zhao, *Chem. Eng. J.*, 2018, **334**, 882–890.
37 X. Yan, J. Deng, J. Xu, H. Li, L. Wang, D. Chen and J. Xie, *Sens. Actuators, B*, 2012, **171–172**, 1087–1094.
38 G. Dykstra, I. Chapa and Y. Liu, *ACS Appl. Mater. Interfaces*, 2014, **16**, 66921–66931.
39 B. L. Li, J. H. Luo, H. Q. Luo and N. B. Li, *Sens. Actuators, B*, 2013, **186**, 96–102.
40 M. W. Glasscott, K. J. Vannoy, R. Kazemi, M. D. Verber and J. E. Dick, *Environ. Sci. Technol. Lett.*, 2020, **7**, 489–495.
41 Z. Wang, Z. Chen, Z. Ma and H. Han, *Anal. Chem.*, 2024, **96**, 14298–14305.
42 G. Bolat, Y. T. Yaman and S. Abaci, *Sens. Actuators, B*, 2019, **299**, 127000.